minerals

MDPI

Article

Effective-Medium Inversion of Induced Polarization Data for Mineral Exploration and Mineral Discrimination: Case Study for the Copper Deposit in Mongolia

Michael Zhdanov [1,2], Masashi Endo [1,*], Leif Cox [1] and David Sunwall [1]

[1] TechnoImaging, Salt Lake City, UT 84107, USA; mzhdanov@technoimaging.com (M.Z.); leif@technoimaging.com (L.C.); david@technoimaging.com (D.S.)

[2] Department of Geology and Geophysics, The University of Utah, Salt Lake City, UT 84112, USA

* Correspondence: masashi@technoimaging.com; Tel.: +1-801-264-6700

Received: 30 November 2017; Accepted: 7 February 2018; Published: 14 February 2018

Abstract: This paper develops a novel method of 3D inversion of induced polarization (IP) survey data, based on a generalized effective-medium model of the IP effect (GEMTIP). The electrical parameters of the effective-conductivity model are determined by the intrinsic petrophysical and geometrical characteristics of composite media, such as the mineralization and/or fluid content of rocks and the matrix composition, porosity, anisotropy, and polarizability of formations. The GEMTIP model of multiphase conductive media provides a quantitative tool for evaluation of the type of mineralization, and the volume content of different minerals using electromagnetic (EM) data. The developed method takes into account the nonlinear nature of both electromagnetic induction and IP phenomena and inverts the EM data in the parameters of the GEMTIP model. The goal of the inversion is to determine the electrical conductivity and the intrinsic chargeability distributions, as well as the other parameters of the relaxation model simultaneously. The recovered parameters of the relaxation model can be used for the discrimination of different rocks, and in this way may provide an ability to distinguish between uneconomic mineral deposits and zones of economic mineralization using geophysical remote sensing technology.

Keywords: effective-medium; induced polarization; 3D inversion

1. Introduction

The induced polarization (IP) effect is caused by the complex electrochemical reactions that accompany current flow in the earth. These reactions take place in a heterogeneous medium representing the rock formations in areas of mineralization. It was demonstrated almost forty years ago in the pioneering papers [1–4] that the IP effect may be used to separate the responses of economic polarized targets from other anomalies. However, until recently, this idea had very limited practical application because of the difficulties in recovering the induced polarization parameters from the observed electromagnetic (EM) data, especially in the case of the 3D interpretation required for efficient exploration of the mining targets.

The quantitative interpretation of IP data in a complex 3D environment is a very challenging problem. The most widely used approach to solving this problem, which is considered the industry standard, was developed by the University of British Columbia's Geophysical Inversion Facility (UBC-GIF). This approach is based on an assumption that the chargeability is relatively small and the IP data can be expressed as a linear functional of the intrinsic chargeability [5,6]. The corresponding linear inverse problem is then solved to obtain the chargeability model under an assumption that the data are not affected by EM coupling. The main limitation of this linearized approach is that it ignores

the nonlinear effects which are significant in IP phenomena. Also, it is impossible to use a linearized approach if we need to recover not just the chargeability, but other parameters of the conductivity relaxation model.

Indeed, a comprehensive analysis of IP phenomena has to be based on models with frequency-dependent complex conductivity distribution. One of the most popular models is the Cole–Cole relaxation model [7]. This model was introduced for studying the IP effect in the pioneering papers [3,4,8]. The Cole–Cole model has been used in a number of publications for the interpretation of IP data (e.g., [9–13]). The parameters of the conductivity relaxation model can be used for discrimination of the different types of rock formations, which is an important goal in mineral and petroleum exploration [1]. It was demonstrated by [14] that the Cole–Cole model can be derived analytically from the general formulas of the generalized effective-medium theory of induced polarization (GEMTIP) in a case of conductive media with spherical polarized inclusions.

Until recently, the Cole–Cole model parameters have been determined mostly in the physical lab by direct analysis of the rock samples. However, [12,15] developed the methods of determining a 3D distribution of the four parameters of the Cole–Cole model based on field IP data.

At the same time, it was demonstrated in [14] that a GEMTIP model, based on a rigorous physical-mathematical description of heterogeneous conductive media using effective-medium theory, provides a more accurate representation of the IP phenomenon than the Cole–Cole model, while GEMTIP is equivalent to the Cole–Cole model for a simple case of spherical inclusions. The electrical parameters of the new composite conductivity model are determined by the intrinsic petrophysical and geometrical characteristics of composite media, such as the mineralization and/or fluid content of rocks and the matrix composition, porosity, anisotropy, and polarizability of formations. The new GEMTIP model of multiphase conductive media provides a quantitative tool for evaluation of the type of mineralization, and the volume content of different minerals using EM data. The practical effectiveness of the GEMTIP model was demonstrated in the recent publications [16,17] by comparison of the resistivity spectra of rock samples and the mineralogical analyses of the same samples using QEMScan electron microscopy technology. The publications cited above have also developed the GEMTIP rock models with elliptical grains and applied these models to studying the complex resistivity of typical mineral rocks.

In this paper, we introduce a novel method of 3D inversion of the IP data based on the GEMTIP conductivity relaxation model with elliptical grains. The developed method takes into account the nonlinear nature of both electromagnetic induction and IP phenomena and inverts the EM data in the parameters of the GEMTIP model. The goal of the inversion is to determine the electrical conductivity and the intrinsic chargeability distributions, as well as the other parameters of the relaxation model simultaneously. The recovered parameters of the relaxation model can be used for the discrimination of different rocks, and in this way may provide an ability to distinguish between uneconomic mineral deposits and zones of economic mineralization using geophysical remote sensing technology.

The solution of this problem requires the development of effective numerical methods for both EM forward modeling and inversion in inhomogeneous media. These problems are extremely difficult, especially in three-dimensional cases. The difficulties arise even in the forward modeling because of the huge size of the numerical problem to be solved to adequately represent the complex 3D distribution of EM parameters of the media, required in mining exploration. As a result, the time and the memory requirements of the computer simulation could be excessive even for practically realistic models. Our approach is based on applying parallel computing for modeling and inversion. Additional difficulties are related to inversion for GEMTIP parameters. This problem is nonlinear and ill posed, because, in general, the solution can be unstable and non-unique. In order to overcome these difficulties, we use the methods of regularization theory to obtain a stable, unique solution of the original ill-posed EM inverse problem [18,19]. We use the integral equation (IE) method for forward modeling and the re-weighted regularized conjugate gradient (RRCG) method for the inversion, which have proved to be effective techniques in geophysical applications [20].

We applied the developed novel method of 3D inversion of the IP data for the comprehensive interpretation of geophysical survey data collected in Mongolia for exploration of a mineral deposit.

2. Regularized Integral Equation (IE)-Based Inversion for Complex Resistivity

There are several advantages to using the IE method in IP data inversion in comparison with the more traditional finite-difference (FD) approach. First, IE forward modeling requires the calculation of the Green's tensors for the background conductivity model. These tensors can be precomputed only once and saved for multiple use on every iteration of an inversion, which speeds up the computation of the predicted data [21]. Finally, IE forward modeling and inversion require the discretization of the domain of inversion only, while in the framework of the FD method one has to discretize the entire modeling domain, which includes not only the area of investigation but an additional domain surrounding this area (including the areas in the air as well). For this reason, the IE inversion method requires just one forward modeling on every iteration step, which speeds up the computations and results in a relatively fast but rigorous inversion method. To obtain a stable solution of a 3D inverse problem, we apply a regularization method based on a focusing stabilizing functional [18]. This stabilizer helps generate a sharp and focused image of the anomalous conductivity distribution, which is important in mineral exploration with the goal of delineating the boundaries of a prospective target.

We know that the EM field recorded at the receiver can be represented as a sum of the background EM field, $\mathbf{E}^b, \mathbf{H}^b$ and the anomalous EM field, $\mathbf{E}^a, \mathbf{H}^a$:

$$\mathbf{E} = \mathbf{E}^b + \mathbf{E}^a, \tag{1}$$

$$\mathbf{H} = \mathbf{H}^b + \mathbf{H}^a. \tag{2}$$

The anomalous electromagnetic field is related to the electric current induced in the inhomogeneity, $j = \Delta\sigma\mathbf{E}$, according to the following integral formulas [18]:

$$\mathbf{E}^a(\mathbf{r}_j) = \int\int\int_D \widehat{\mathbf{G}}_E(\mathbf{r}_j\,|\mathbf{r}\,)\cdot\Delta\sigma(\mathbf{r})\mathbf{E}(\mathbf{r})dv = \mathbf{G}_E\left[\Delta\sigma\mathbf{E}\right], \tag{3}$$

$$\mathbf{H}^a(\mathbf{r}_j) = \int\int\int_D \widehat{\mathbf{G}}_H(\mathbf{r}_j\,|\mathbf{r}\,)\cdot\Delta\sigma(\mathbf{r})\mathbf{H}(\mathbf{r})dv = \mathbf{G}_H\left[\Delta\sigma\mathbf{H}\right], \tag{4}$$

where $\widehat{\mathbf{G}}_E(\mathbf{r}_j\,|\mathbf{r}\,)$ and $\widehat{\mathbf{G}}_H(\mathbf{r}_j\,|\mathbf{r}\,)$ are the electric and magnetic Green's tensors defined for an unbounded conductive medium with the background (horizontally-layered) conductivity σ_b; $\mathbf{G}_E$ and $\mathbf{G}_H$ are the corresponding Green's linear operators; and domain D represents a volume with an arbitrary varying conductivity, $\sigma_a = \sigma_b + \Delta\sigma_a$, within a domain D.

By using both integral Equations (3) and (4), we vastly simplify both the forward and inverse problems of the IP method. Our problem can now be written in the classic form of the operator equation:

$$\mathbf{d} = A(\Delta\sigma), \tag{5}$$

where $\Delta\sigma$ is a vector formed by the anomalous conductivities within the targeted domain. The inversion is based on minimization of the Tikhonov parametric functional, $P^\alpha(\Delta\sigma)$, with the corresponding stabilizer $S(\Delta\sigma)$ [22]:

$$P^\alpha(\Delta\sigma) = \|\mathbf{W}_d(A(\Delta\sigma) - \mathbf{d}\|^2_{L_2} + \alpha S(\Delta\sigma), \tag{6}$$

where $\mathbf{W}_d$ is the data weighting matrix, and α is a regularization parameter (used to balance the misfit and stabilizer terms in Equation (6)). By minimizing parametric functional $P^\alpha(\Delta\sigma)$, we can find the solution of the inverse problem. A standard technique to find a minimum of $P^\alpha(\Delta\sigma)$ is to apply a gradient type minimization method [18,19]. We use the regularized conjugate gradient method

(RCGM) to find the solution of the inverse problem. The mathematical outline of the RCGM method is as follows:

$$\mathbf{r}_n = A(\mathbf{m}_n) - \mathbf{d}, \qquad (a)$$

$$\mathbf{l}_n^{\alpha_n} = \mathbf{l}^{\alpha_n}(\mathbf{m}_n) = \mathbf{F}_n^T \mathbf{W}_d^2 \mathbf{r}_n + \alpha_n \mathbf{W}_m^2 (\mathbf{m}_n - \mathbf{m}_{apr}), \qquad (b)$$

$$\beta_n^{\alpha_n} = \left\|\mathbf{l}_n^{\alpha_n}\right\|^2 / \left\|\mathbf{l}_{n-1}^{\alpha_{n-1}}\right\|^2, \quad \tilde{\mathbf{l}}_n^{\alpha_n} = \mathbf{l}_n^{\alpha_n} + \beta_n^{\alpha_n} \tilde{\mathbf{l}}_{n-1}^{\alpha_{n-1}}, \; \tilde{\mathbf{l}}_0^{\alpha_0} = \mathbf{l}_0^{\alpha_0}, \; (c) \qquad (7)$$

$$\tilde{k}_n^{\alpha_n} = \left(\tilde{\mathbf{l}}_n^{\alpha_n T} \mathbf{l}_n^{\alpha_n}\right) / \left\{ \left\|\mathbf{W}_d \mathbf{F}_n \tilde{\mathbf{l}}_n^{\alpha_n}\right\|^2 + \alpha \left\|\mathbf{W}_m \tilde{\mathbf{l}}_n^{\alpha_n}\right\|^2 \right\}, \quad (d)$$

$$\mathbf{m}_{n+1} = \mathbf{m}_n - \tilde{k}_n^{\alpha_n} \tilde{\mathbf{l}}_n^{\alpha_n}, \qquad (e)$$

where $\mathbf{W}_m$ is the weighting matrix of the model parameters, and $\mathbf{F}_n$ is the matrix of the Fréchet derivative of the forward modeling operator A.

The iterative process (7) is terminated when the misfit reaches the given level of noise in the data, ε_0 :

$$\phi(\mathbf{m}_N) = \|\mathbf{r}_N\|^2 \le \varepsilon_0^2.$$

3. GEMTIP Resistivity Relaxation Model

In a general case, the effective conductivity of rocks is not necessarily a constant and real number, but is complex and may vary with frequency. A general approach to constructing the resistivity relaxation model is based on the rock physics and description of the medium as a composite heterogeneous multiphase formation [14].

In the paper [16], we introduced for simplicity, the frequency-dependant complex resistivity for a two-phase model with elliptical inclusions, described by the following formula

$$\rho_e = \rho_0 \left\{ 1 + \frac{f}{3} \sum_{\alpha=x,y,z} \frac{1}{\gamma_\alpha} \left[1 - \frac{1}{1 + s_\alpha (i\omega\tau)^C} \right] \right\}^{-1}, \qquad (8)$$

where ρ_0 is the DC resistivity (Ω·m); ω is the angular frequency (rad/s); τ is the time parameter, and C is the relaxation parameter. The coefficients γ_α and s_α ($\alpha = x, y, z$) are the structural coefficients defined by geometrical characteristics of the ellipsoidal inclusions used to approximate the grains:

$$s_\alpha = r_\alpha / \bar{a}, \qquad (9)$$

and $\bar{a}$ is an average value of the equatorial (a_x and a_y) and polar (a_z) radii of the ellipsoidal grains, i.e.,

$$\bar{a} = \frac{(a_x + a_y + a_z)}{3}, \qquad (10)$$

$$r_\alpha = 2\frac{\gamma_\alpha}{\lambda_\alpha}, \qquad (11)$$

where γ_α and λ_α are the diagonal components of the volume and surface depolarization tensors described in [16].

In the case of spherical inclusions of radius a, $\gamma_\alpha = 1/3$, $\lambda_\alpha = 2/3a$, $r_\alpha = a$, and $s_\alpha = 1$, for $\alpha = x, y, z$. Therefore, Formula (8) can be simplified a follows:

$$\rho_e = \rho_0 \left\{ 1 + 3f \left[1 - \frac{1}{1 + (i\omega\tau)^C} \right] \right\}^{-1}. \qquad (12)$$

After some algebra, we can transform Formula (12) in a form similar to the conventional Cole–Cole formula for the effective resistivity:

$$\rho(\omega) = \rho\left(1 - \eta\left(1 - \frac{1}{1 + (i\omega\tau)^{\mathrm{C}}}\right)\right), \tag{13}$$

where ρ is the DC resistivity (Ω·m); ω is the angular frequency (rad/s), τ is the time parameter; η is the intrinsic chargeability, and C is the relaxation parameter. The dimensionless intrinsic chargeability, η, characterizes the intensity of the IP effect.

However, the inversion will be run with respect to the conductivity; therefore, it is more convenient to express the conductivity using Formula (12):

$$\sigma(\omega) = \sigma\left(1 + 3f\left(1 - \frac{1}{1 + (i\omega\tau)^{\mathrm{C}}}\right)\right), \tag{14}$$

In this case, the anomalous conductivity, $\Delta\widetilde{\sigma}$, is equal to

$$\Delta\widetilde{\sigma} = \sigma(\omega) - \sigma_b. \tag{15}$$

Thus

$$\Delta\widetilde{\sigma} = \sigma f\left(\eta, \tau, \mathrm{C}\right) - \sigma_b = \sigma\left(1 + 3f\left(1 - \frac{1}{1 + (i\omega\tau)^{\mathrm{C}}}\right)\right) - \sigma_b, \tag{16}$$

where function $f\left(\eta, \tau, \mathrm{C}\right)$ is equal

$$f\left(\eta, \tau, \mathrm{C}\right) = \left(1 + 3f\left(1 - \frac{1}{1 + (i\omega\tau)^{\mathrm{C}}}\right)\right). \tag{17}$$

4. Regularized Inversion for the GEMTIP Model Parameters

We have demonstrated above that, in the case of the IP effect, the conductivity becomes a complex and frequency-dependent function, $\sigma = \sigma(\omega)$, which increases significantly the number of unknown parameters of the inversion. We can reduce this number by approximating the conductivity relaxation curve using, for example, a GEMTIP model (14).

Indeed, let us substitute expression (16) for the anomalous conductivity into operator Equation (5):

$$\mathbf{d} = A(\sigma f\left(\eta, \tau, \mathrm{C}\right) - \sigma_b) = A_G\left(\mathbf{m}\right), \tag{18}$$

where A_G is a GEMTIP forward modeling operator, and $\mathbf{m}$ is a vector of the GEMTIP model parameters $[\sigma, \eta, \tau, C]$.

We can reformulate now the inverse problem with respect to the GEMTIP model parameters $\mathbf{m}$.

The inversion, as above, is based on minimization of the Tikhonov parametric functional, $P^{\alpha}(\mathbf{m})$, with the corresponding stabilizer $S(m)$ [22]:

$$P^{\alpha}(\mathbf{m}) = \|\mathbf{W}_d(A_G(\mathbf{m}) - \mathbf{d}\|^2_{L_2} + \alpha S(\mathbf{m}). \tag{19}$$

where $\mathbf{W}_d$ is the data-weighting matrix, and α is a regularization parameter. There are several possible choices for the stabilizer [18,19]. In the current paper, for simplicity, we use the minimum norm stabilizer (S_{MN}), which is equal to the square L_2 norm of the difference between the current model $\mathbf{m}$ and an appropriate a priori model $\mathbf{m}_{apr}$:

$$S_{MN}(\mathbf{m}) = \|\mathbf{W}_m(\mathbf{m} - \mathbf{m}_{apr})\|^2_{L_2},$$

where $\mathbf{W}_m$ is the weighting matrix of the model parameters.

The most common approach to minimization of the parametric functional $P(\mathbf{m})$ is based on using gradient-type methods. For example, we provided a summary of the regularized conjugate gradient (RCG) algorithm of the parametric functional minimization in expression (7) above.

The appropriate selection of the data and model parameters weighting matrices is very important for the success of the inversion. We determine the data weights as a diagonal matrix formed by the inverse absolute values of the background field. Computation of the model weighting matrix, $\mathbf{W}_m$, is based on sensitivity analysis. In the current paper, we select $\mathbf{W}_m$ as the square root of the sensitivity matrix for the model in each iteration:

$$\mathbf{W}_m^{(n)} = \sqrt{\text{diag}\left(\mathbf{F}_{m_n}^{*}\mathbf{F}_{m_n}^{*}\right)}.$$

As a result, we obtain a uniform sensitivity of the data to different model parameters [19].

We apply the adaptive regularization method. The regularization parameter α is updated in the process of the iterative inversion as follows:

$$\alpha_n = \alpha_1 q^{n-1};\ n = 1,2,3,\cdots;\ 0 < q < 1.$$

In order to avoid divergence, we begin an iteration from a value of α_1, which can be obtained as a ratio of the misfit functional and the stabilizer for an initial model, then reduce α_n according to the last formula on each subsequent iteration and continuously iterate until the misfit condition is reached:

$$r_{n0}^{w} = \|\mathbf{r}_{n0}^{w}\| = \| \mathbf{W}_d \left[\mathbf{A}\left(\mathbf{m}_{\alpha_{n0}}\right) - \mathbf{d}\right] \| \ / \ \|\mathbf{W}_d\mathbf{d}\| \le \delta, \tag{20}$$

where r_{n0}^{w} is the normalized weighted residual, and δ is the relative level of noise in the weighted observed data.

5. Fréchet Derivative Calculation Using the Quasi-Born Approximation

We assume, as above, that the conductivity within a 3D geoelectrical model can be presented by the background (horizontally layered) conductivity σ_b, and an arbitrary varying conductivity, $\sigma_a = \sigma_b + \Delta\sigma_a$, within a domain D.

In this model, the anomalous field is produced by the anomalous conductivity distribution $\Delta\sigma_a$, and it can be calculated according to Formulas (3) and (4). Using these integral representations, we can express the corresponding Fréchet derivatives, $\mathbf{F}_E$ and $\mathbf{F}_H$, as follows:

$$\begin{aligned}
\mathbf{F}_E\left(\mathbf{r}_j|\mathbf{r}\right) &= \left.\frac{\partial \mathbf{E}\left(\mathbf{r}_j\right)}{\partial\Delta\sigma_a\left(\mathbf{r}\right)}\right|_{\Delta\sigma_a} = \left.\frac{\partial \mathbf{E}^{\Delta\sigma_a}\left(\mathbf{r}_j\right)}{\partial\Delta\sigma_a\left(\mathbf{r}\right)}\right|_{\Delta\sigma_a} = \left.\frac{\partial \mathbf{G}_E\left(\mathbf{r}_j|\mathbf{r}\right)\left[\Delta\sigma_a\left(\mathbf{r}\right)\mathbf{E}\left(\mathbf{r}\right)\right]}{\partial\Delta\sigma_a\left(\mathbf{r}\right)}\right|_{\Delta\sigma_a}, \\
\mathbf{F}_H\left(\mathbf{r}_j|\mathbf{r}\right) &= \left.\frac{\partial \mathbf{H}\left(\mathbf{r}_j\right)}{\partial\Delta\sigma_a\left(\mathbf{r}\right)}\right|_{\Delta\sigma_a} = \left.\frac{\partial \mathbf{H}^{\Delta\sigma_a}\left(\mathbf{r}_j\right)}{\partial\Delta\sigma_a\left(\mathbf{r}\right)}\right|_{\Delta\sigma_a} = \left.\frac{\partial \mathbf{G}_H\left(\mathbf{r}_j|\mathbf{r}\right)\left[\Delta\sigma_a\left(\mathbf{r}\right)\mathbf{E}\left(\mathbf{r}\right)\right]}{\partial\Delta\sigma_a\left(\mathbf{r}\right)}\right|_{\Delta\sigma_a}.
\end{aligned}$$

We can treat the electric field $\mathbf{E}^{(n)}\left(\mathbf{r}\right)$, found on iteration number n, as the electric field in the above equations for a subsequent iteration $(n+1)$, $\mathbf{E}\left(\mathbf{r}\right) = \mathbf{E}^{(n)}\left(\mathbf{r}\right)$. In this case, the Fréchet derivatives at iteration number n can be found by direct integration from the last two equations involving the electric field $\mathbf{E}^{(n)}\left(\mathbf{r}\right)$ computed on the current iteration:

$$\mathbf{F}_{E,H}\left(\mathbf{r}_j|\mathbf{r}\right) = \left.\frac{\partial \mathbf{G}_{E,H}\left(\mathbf{r}_j|\mathbf{r}\right)\left[\Delta\sigma_a\left(\mathbf{r}\right)\mathbf{E}\left(\mathbf{r}\right)\right]}{\partial\Delta\sigma_a\left(\mathbf{r}\right)}\right|_{\Delta\sigma_a} \approx \mathbf{G}_{E,H}\left(\mathbf{r}_j|\mathbf{r}\right)\mathbf{E}^{(n)}\left(\mathbf{r}\right).$$

Note that, the electric field $\mathbf{E}^{(n)}\left(\mathbf{r}\right)$ is calculated using the rigorous IE forward modeling method at each iteration step to compute the predicted data (EM field at the receivers). Therefore, no extra computation is required to find the electric field for the Fréchet derivative calculation.

In the case of time domain EM data, the Fréchet derivatives also need to be transformed into time domain. This can be accomplished by the same technique as that for EM fields, i.e., by the Fourier transform using digital filtering techniques. For example, in the case of a causal step turnoff response, the Fréchet derivative in time domain can be expressed as follows:

$$\mathbf{f}_{E,H}(t) = -\frac{2}{\pi}\int_0^\infty \frac{\mathrm{Im}\left[\mathbf{F}_{E,H}(\omega)\right]}{\omega}\cos(\omega t)\,d\omega.$$

As a result, our inversion technique, based on the IE method, requires just one forward modeling on every iteration step, while the conventional inversion scheme requires, as a rule, at least three forward modeling solutions per inversion iteration (one to compute the predicted data, another one to compute the gradient direction, and at least one for optimal calculation of the iteration step). This approach results in a very efficient inversion method.

6. Calculation of the Fréchet Derivatives with Respect to the GEMTIP Model Parameters

In the current project, we consider the GEMTIP model describing a two-phase composite medium. This GEMTIP model is characterized by four parameters (conductivity of the host medium, σ_0, fraction volume f, time constant, τ, and relaxation coefficient, C). Therefore, the Fréchet derivatives, with respect to each GEMTIP parameter, are required to invert the IP data.

The Fréchet derivative of the EM fields with respect to the conductivity of the host medium can be computed as follows:

$$\begin{aligned}\mathbf{F}^{\sigma_0}_{E,H}(\mathbf{r}_j|\mathbf{r}) &= \mathbf{F}^{\sigma_e}_{E,H}(\mathbf{r}_j|\mathbf{r})\cdot\frac{\partial\sigma_e}{\partial\sigma_0},\\ \frac{\partial\sigma_e}{\partial\sigma_0} &= 1+\frac{f}{3}\left\{1-\frac{1}{1+(i\omega\tau)^C}\right\}.\end{aligned}$$

The Fréchet derivative of the EM fields, with respect to the fraction volume, can be computed as follows:

$$\begin{aligned}\mathbf{F}^{f}_{E,H}(\mathbf{r}_j|\mathbf{r}) &= \mathbf{F}^{\sigma_e}_{E,H}(\mathbf{r}_j|\mathbf{r})\cdot\frac{\partial\sigma_e}{\partial f},\\ \frac{\partial\sigma_e}{\partial f} &= \frac{\sigma_0}{3}\left\{1-\frac{1}{1+(i\omega\tau)^C}\right\}.\end{aligned}$$

The Fréchet derivative of the EM fields, with respect to the time constant, can be determined as:

$$\begin{aligned}\mathbf{F}^{\tau}_{E,H}(\mathbf{r}_j|\mathbf{r}) &= \mathbf{F}^{\sigma_e}_{E,H}(\mathbf{r}_j|\mathbf{r})\cdot\frac{\partial\sigma_e}{\partial\tau},\\ \frac{\partial\sigma_e}{\partial\tau} &= \frac{\sigma_0 i\omega C(i\omega\tau)^{C-1}\left\{f/3-(1+f/3)(i\omega\tau)^C\right\}}{\left\{1+(i\omega\tau)^C\right\}^2}.\end{aligned}$$

The Fréchet derivative of the EM fields, with respect to the relaxation coefficient, is equal to:

$$\begin{aligned}\mathbf{F}^{C}_{E,H}(\mathbf{r}_j|\mathbf{r}) &= \mathbf{F}^{\sigma_e}_{E,H}(\mathbf{r}_j|\mathbf{r})\cdot\frac{\partial\sigma_e}{\partial C},\\ \frac{\partial\sigma_e}{\partial C} &= \frac{\sigma_0 f(i\omega\tau)^C\ln(i\omega\tau)}{3\left\{1+(i\omega\tau)^C\right\}^2}.\end{aligned}$$

Note that, in all formulas above, the Fréchet derivative, with respect to the effective conductivity, is given by the following expression:

$$\mathbf{F}^{\sigma_e}_{E,H}\left(\mathbf{r}_j|\mathbf{r}\right) = \frac{\partial \mathbf{G}_{E,H}\left(\mathbf{r}_j|\mathbf{r}\right)\left[\Delta\sigma_e\left(\mathbf{r}\right)\mathbf{E}\left(\mathbf{r}\right)\right]}{\partial\Delta\sigma_e\left(\mathbf{r}\right)}.$$

In order to compute the Fréchet derivatives in the time domain, one can use the Fourier transform, as was discussed above .

7. Model Study of 3D Spectral IP Inversion in the Frequency Domain and in the Time Domain

In order to develop an effective algorithm for 3D inversion of spectral IP data in both the frequency and time domains, a simple synthetic model (as shown in Figure 1) was used. The model contains an IP anomaly, with the conductivity described by a GEMTIP model, embedded in a homogeneous half-space. The parameters of this model are as follows:

- Resistivity of the background (homogeneous half-space): 100 Ω·m
- GEMTIP parameters:

  - Grain size: 1×10^{-4}, 1×10^{-5} m (major and minor radii of ellipsoidal grain)
  - DC resistivity: 5 Ω·m
  - Fraction volume: 33% (Chargeability coefficient: 0.5)
  - Time constant: 1.0 s
  - Relaxation coefficient: 0.5

Dipole–dipole IP surveys were simulated, with electrode spacing $a = 100$ m, and a maximum separation between the current and the potential electrodes of 700 m ($n = 7$). Both frequency and time domain synthetic data were generated, as discussed below.

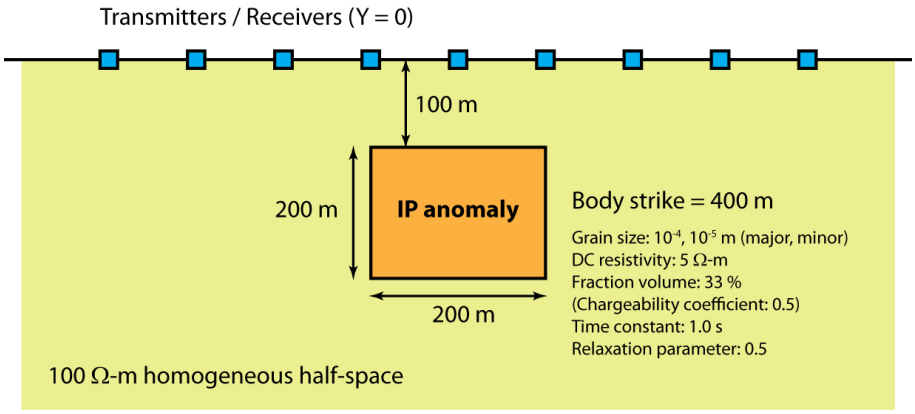

Figure 1. A 3D IP model used for the model study.

7.1. 3D Inversion of Frequency-Domain IP Data

In order to simulate a dipole–dipole SIP survey (in the frequency domain), synthetic data were generated at 15 frequencies (0.125, 0.375, 0.625, 0.875, 1, 1.125, 3, 5, 7, 8, 9, 24, 40, 56 and 72 Hz).

The test results from inversion of the frequency domain synthetic data are shown in Figure 2; this shows vertical cross sections (below the survey line, $Y = 0$ m) of the four 3D GEMTIP model parameters (DC anomalous conductivity, fraction volume, time constant, and relaxation parameter), recovered from the 3D inversion of frequency-domain SIP data. One can see that the spacial distributions and values of the inverted GEMTIP parameters are in good agreement with the true model (shown in white rectangles in Figure 2).

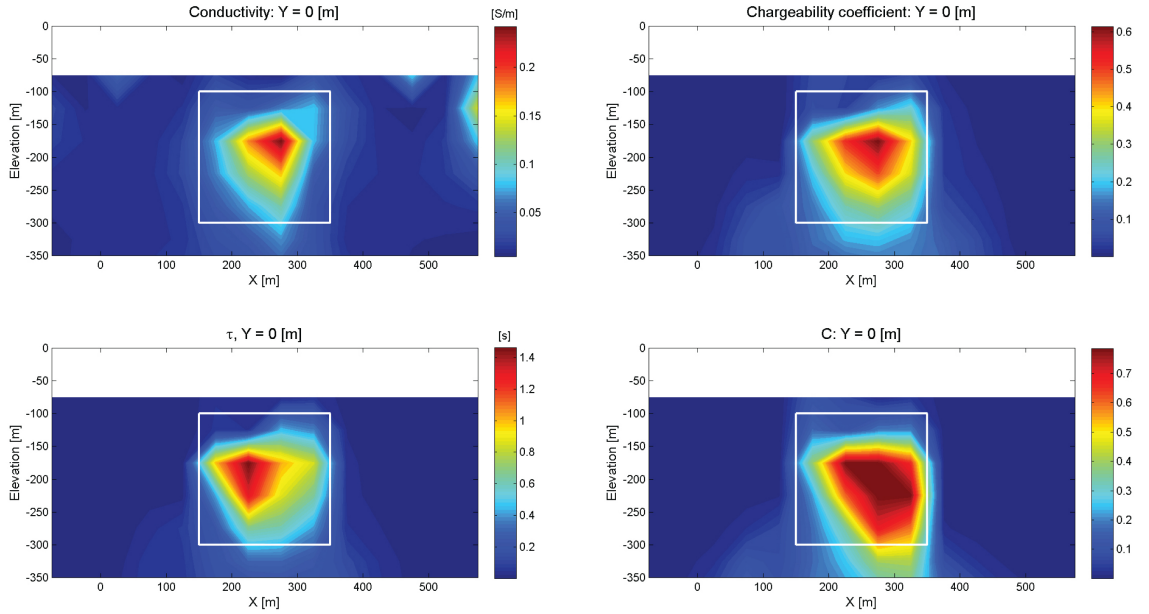

Figure 2. Vertical cross sections of the GEMTIP model parameters (DC anomalous conductivity, fraction volume, time constant, and relaxation parameter) recovered from the 3D inversion of frequency-domain SIP data.

7.2. 3D Inversion of Time-Domain IP Data

In order to simulate a dipole–dipole SIP survey (in the time domain), synthetic data were generated for time-steps from 1×10^{-5} to 0.1 s at 10 points per decade.

Figure 3 shows the vertical cross sections (below the survey line, $Y = 0$ m) of 3D GEMTIP model parameters (DC anomalous conductivity, fraction volume, time constant, and relaxation parameter) recovered using the synthetic time-domain SIP data. Again, there is reasonable agreement with the true model (shown in white rectangles in Figure 3).

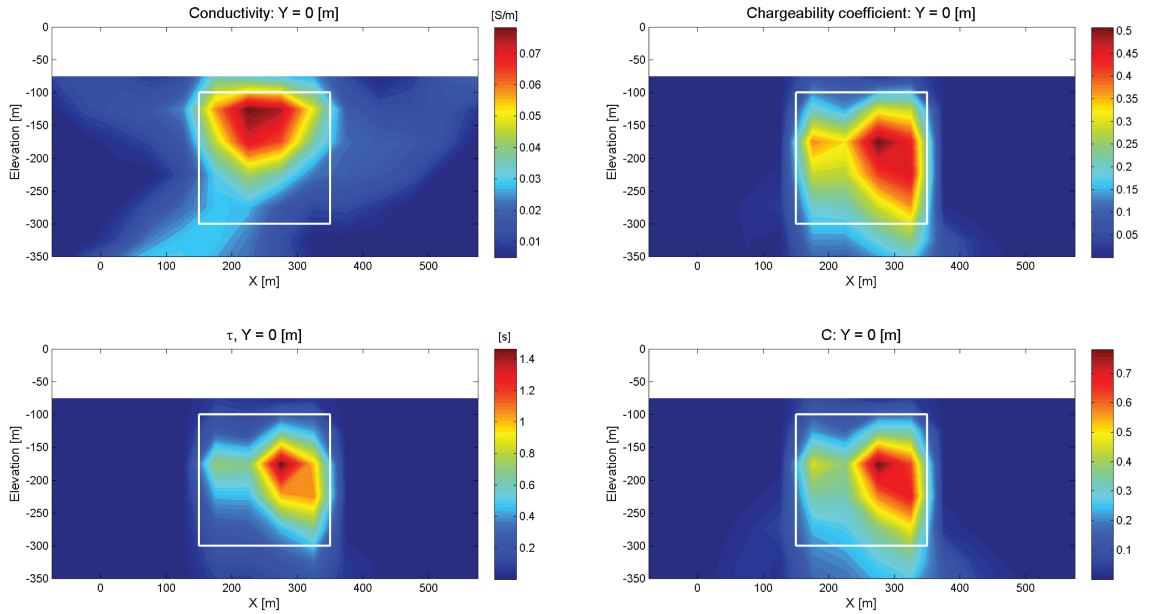

Figure 3. Vertical cross sections of the GEMTIP model parameters (DC anomalous conductivity, fraction volume, time constant, and relaxation parameter) recovered from the 3D inversion of time-domain SIP data.

This model study illustrates that both the frequency-domain and time-domain SIP data contain enough information for the GEMTIP parameters to be recovered from these data. We will illustrate this fact in more detail in the case study presented in the next section.

8. Case Study for the Copper Deposit in Mongolia

Multiple geophysical surveys, which included IP, and magnetic surveys, were carried out in Mongolia. The survey area is located about 1800 km west from Ulan Bator, about 150 km from the Bayan-Ulugii province center (Figure 4). The main objective of this survey was to determine the alteration and mineralization zones.

In order to conduct a comprehensive interpretation of the IP survey data, the petrophysical and mineralogical analyses of rock samples (drill cores) collected in the survey area were also deployed. The following workflow was established for the comprehensive interpretation, in order to build 3D geology/lithology models and to outline the target mineralized zones:

1. 3D inversions of IP data: to produce 3D models of the electrical properties (GEMTIP model parameters);
2. Petrophysical and mineralogical analyses of rock samples: to determine the relationship between geology/lithology and electrical properties;
3. Interpretation of the obtained results: to generate the images of the target mineralized zones (on deposit scale).

The workflow of this comprehensive interpretation is also shown in Figure 5.

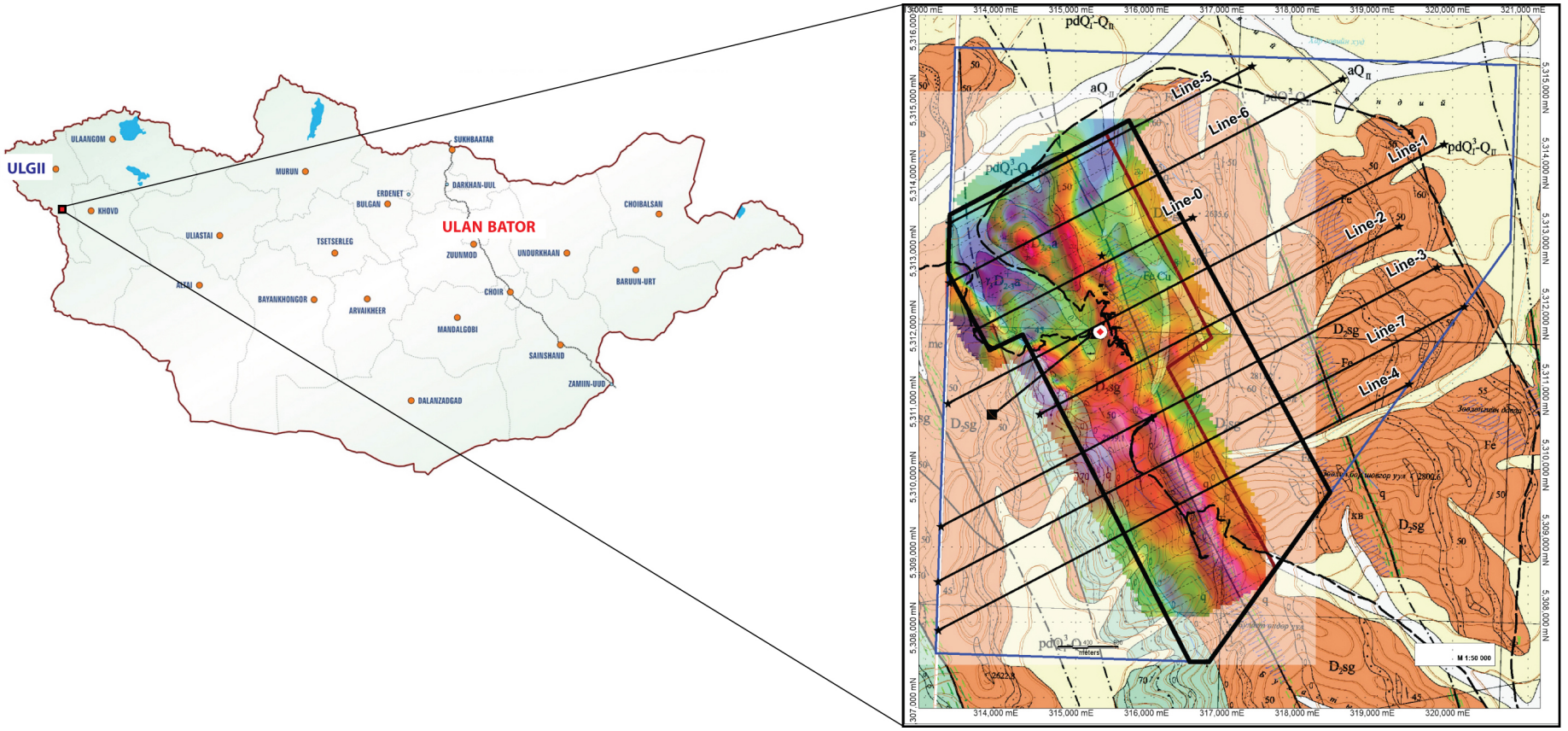

Figure 4. Location map of the geophysical survey area in Mongolia.

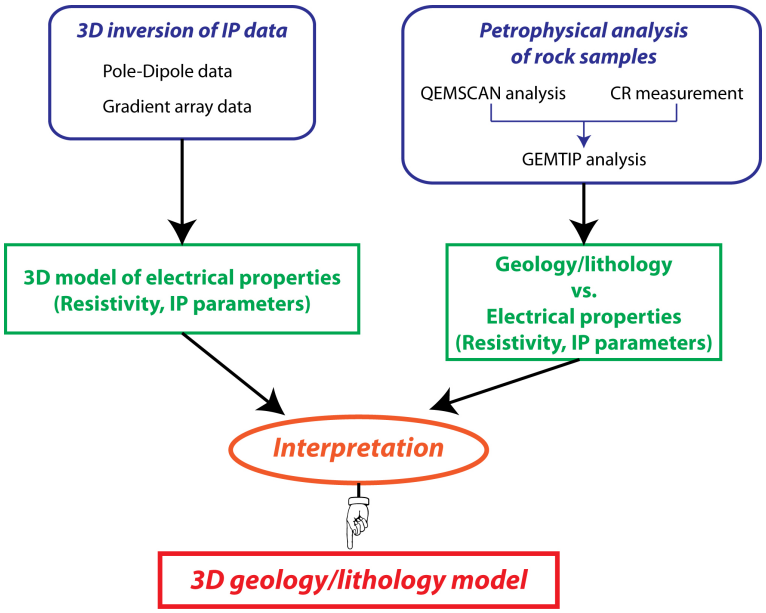

Figure 5. A workflow of the comprehensive interpretation of IP survey data.

8.1. 3D Inversion of IP Data

We have inverted the IP data (time-domain IP data with pole–dipole and gradient electrode arrays) in 3D for the GEMTIP model parameters, DC resistivity, chargeability, time constant, and relaxation parameter. Figure 6 shows the IP survey lines with locations of drill holes in the survey area. In this figure, the black rectangle outlines the area where we show the 3D geoelectrical model recovered from the 3D inversion of IP data (a part of the inversion domain; the area with higher potential of the mineralization, estimated from the drilling results).

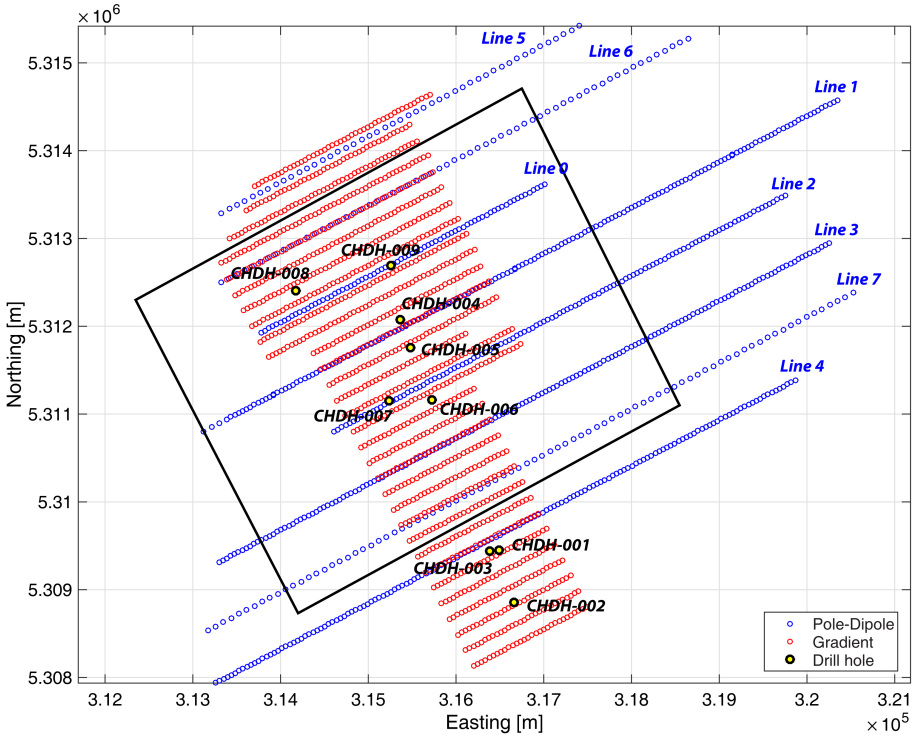

Figure 6. IP survey lines (pole–dipole and gradient arrays) in the survey area. The black rectangle shows the area with higher potential of mineralization, estimated from drilling results.

The specifications of IP surveys are as follows:

1. Pole–Dipole IP survey (time domain)

   - Total of 8 lines (numbered from 0 to 7, shown as blue dots in Figure 6)
   - Transmitter: with two current electrodes (A and B); one of them (A) is located on the survey line, while another (B) is located far from the survey line.
   - Spacing of two potential (receiver) electrodes (M and N, spacing a): 100 and/or 200 m.
   - Period of the transmitting current: 2 s.
   - Data acquisition: from 0.04 to 2 s after the transmitting current is turned off, with semi-logarithmic 20 time windows.

2. Gradient IP survey (time-domain)

   - Total 66-km line (shown as red dots in Figure 6); whole area was divided into three blocks.
   - Transmitter: electric bipole with the length of 1.2 to 3 km.
   - Spacing of two potential (receiver) electrodes: 50 m.
   - Period of the transmitting current: 2 s ON, and 2 s OFF.
   - Data acquisition: from 0.06 to 2 s after the transmitting current is turned off, with semi-logarithmic 20 time windows.

Figure 7 shows an example of the observed and predicted pole–dipole IP data from 3D inversion. One can see the good agreement between the observed and predicted data.

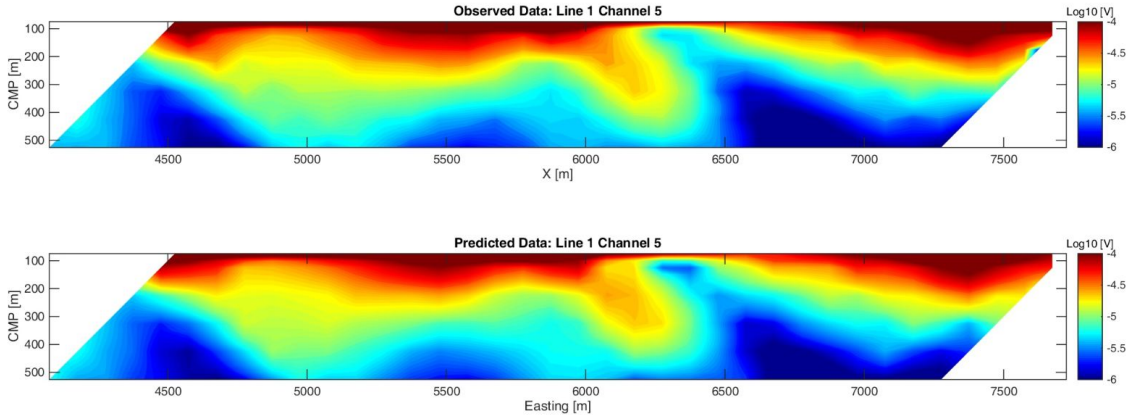

Figure 7. IP survey lines (Pseudo sections of the observed (top) and predicted (bottom) pole–dipole IP data; Line 1, time channel 5.

Figures 8–11 show the 3D distributions of resistivity, chargeability, time constant, and relaxation parameter, recovered from 3D inversion of pole–dipole IP data. Note that the 3D models recovered from the gradient IP data are very similar to the ones recovered from the pole–dipole IP data.

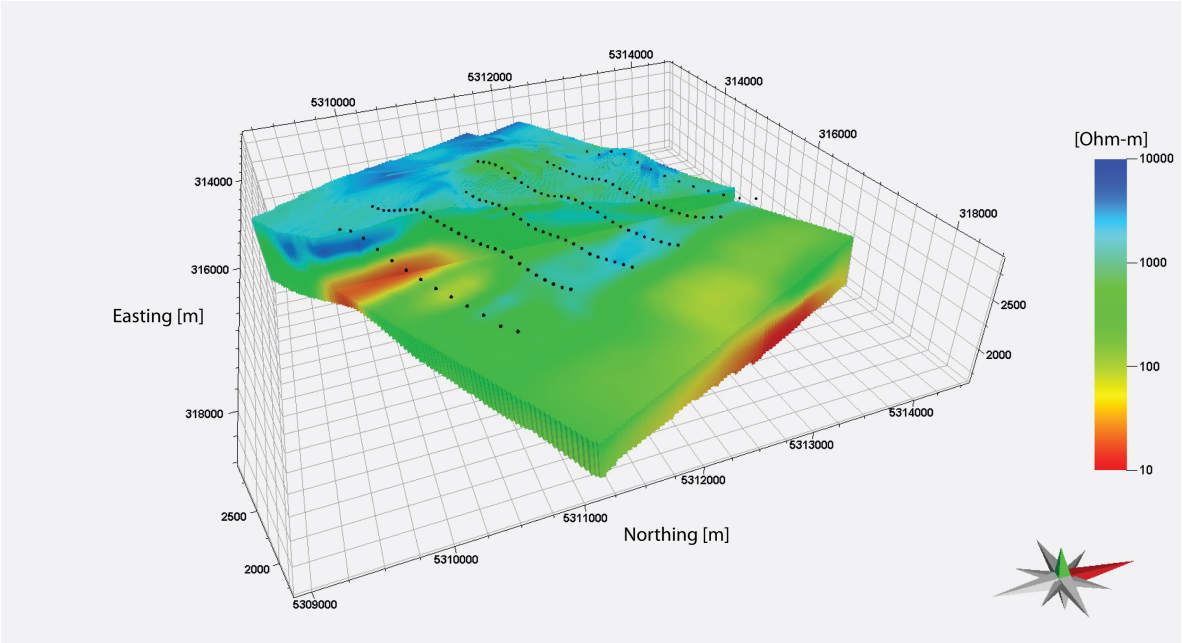

Figure 8. A 3D view of the 3D resistivity model recovered from 3D inversion of pole–dipole IP data.

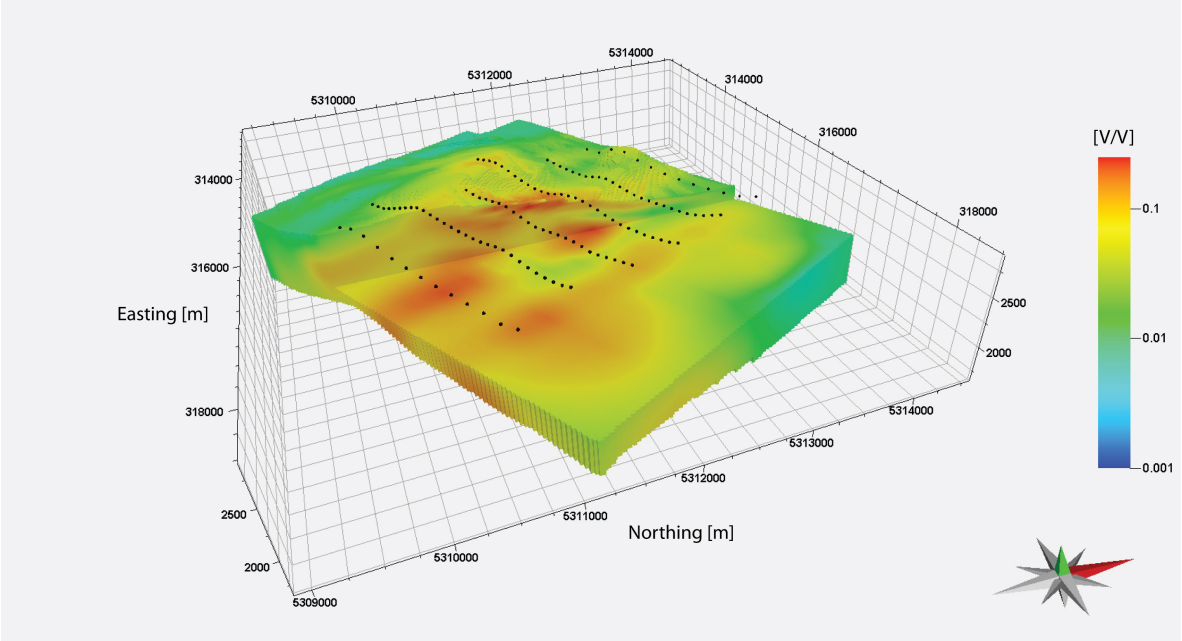

Figure 9. A 3D view of the 3D chargeability model recovered from 3D inversion of pole–dipole IP data.

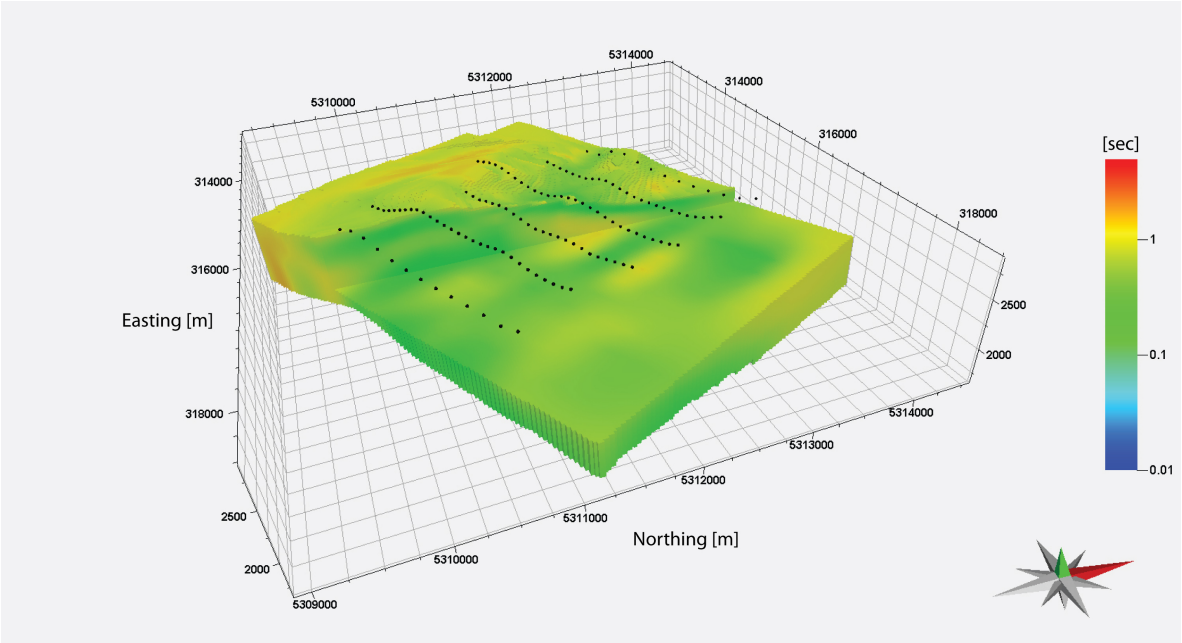

Figure 10. A 3D view of the 3D time constant model recovered from 3D inversion of pole–dipole IP data.

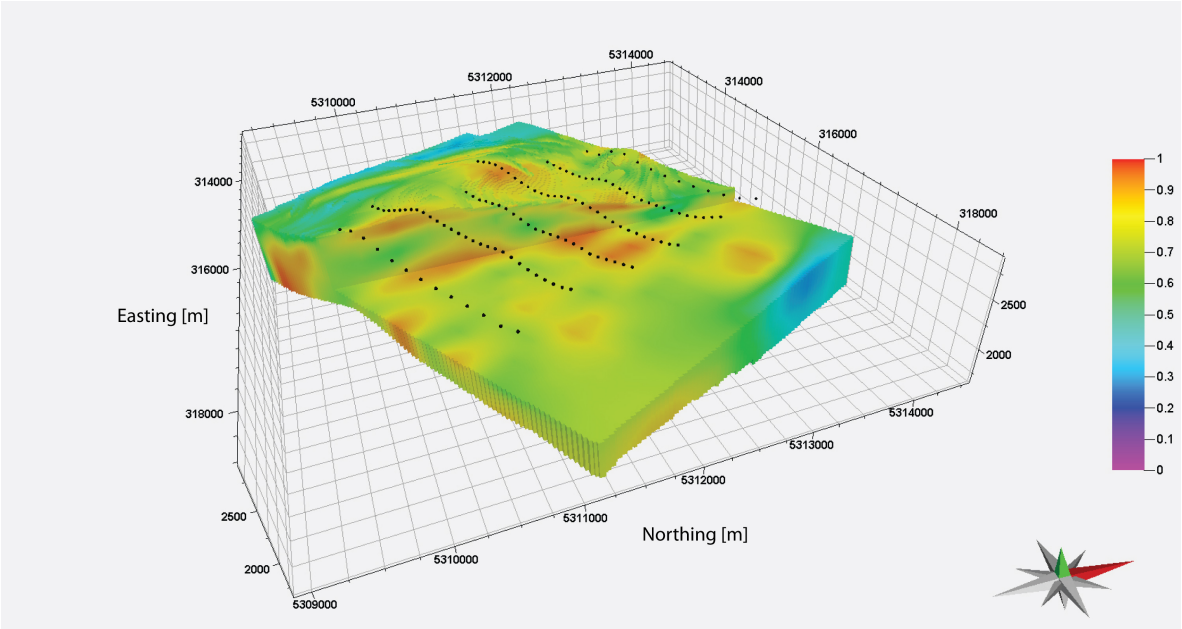

Figure 11. A 3D view of the 3D relaxation parameter model recovered from 3D inversion of pole–dipole IP data.

Figures 12–15 show vertical cross sections of 3D models (resistivity, chargeability, time constant, and relaxation parameter) recovered from 3D inversion of pole–dipole IP data along survey line 1.

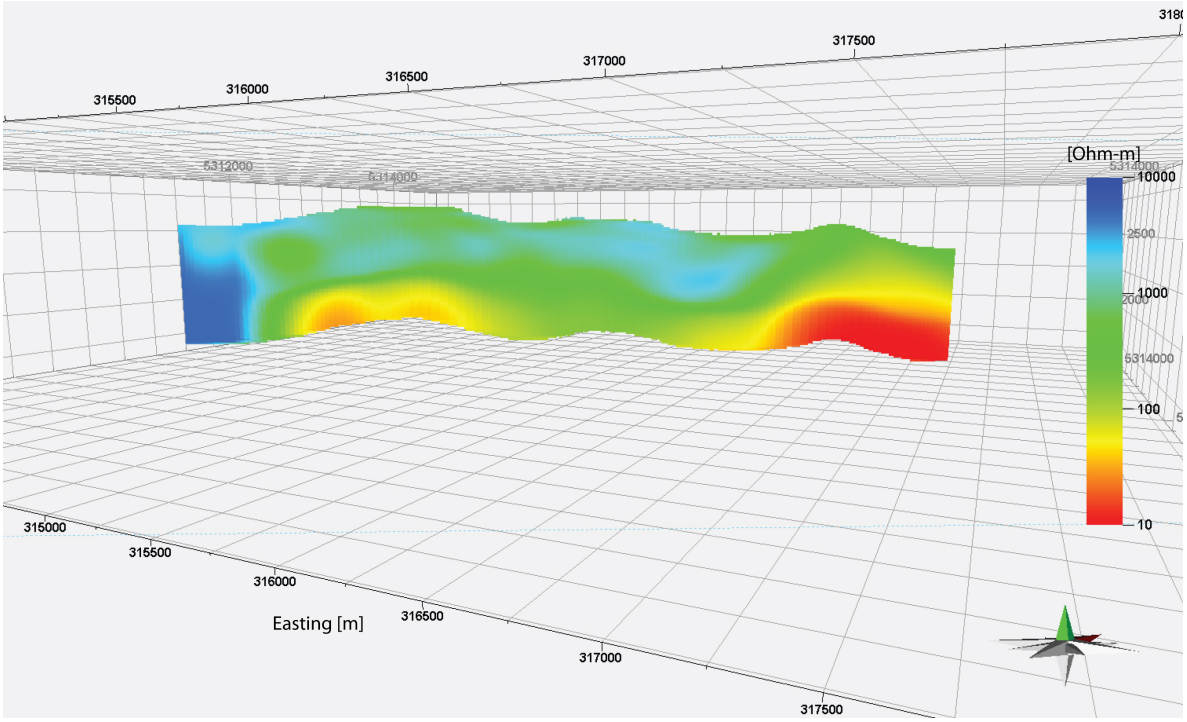

Figure 12. A vertical cross section of the 3D resistivity model recovered from 3D inversion of the pole–dipole IP data along Line 1.

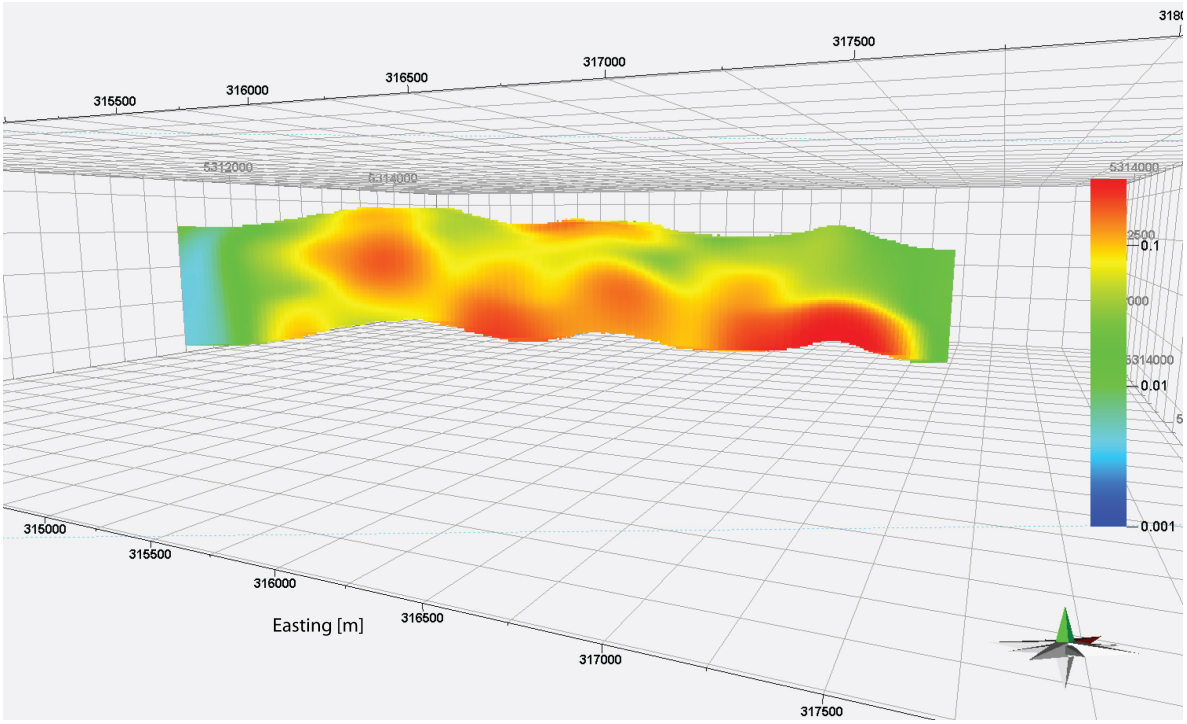

Figure 13. A vertical cross section of the 3D chargeability model recovered from 3D inversion of the pole–dipole IP data along Line 1.

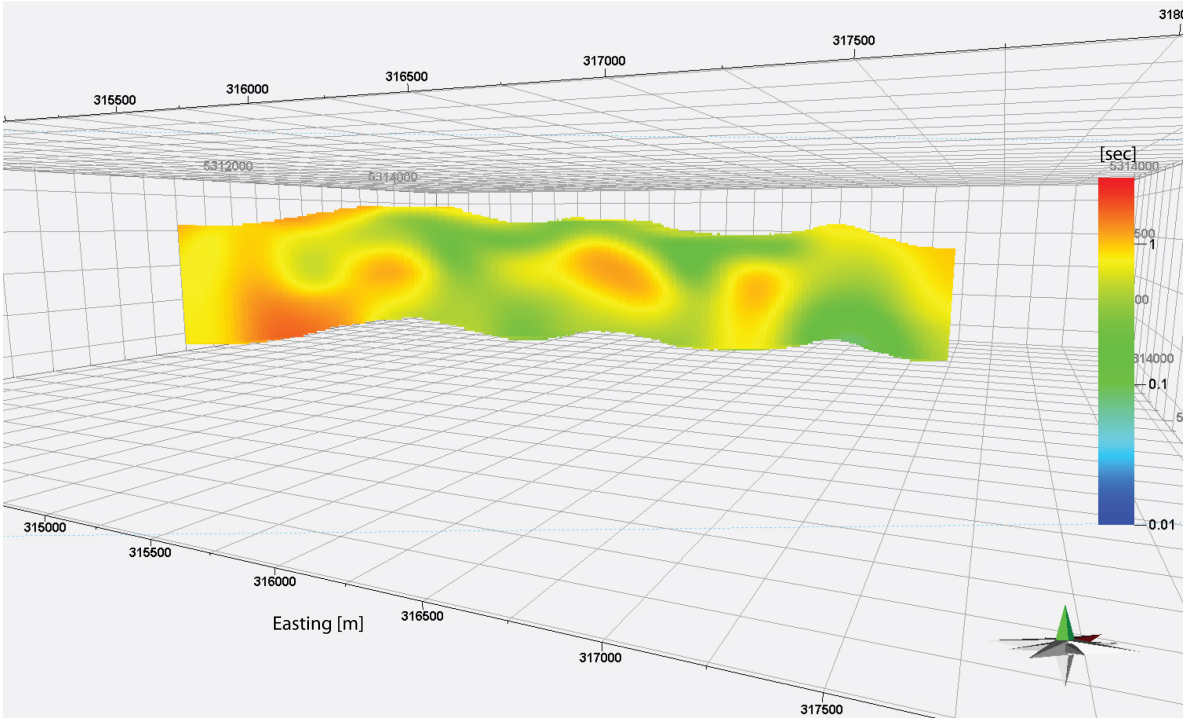

Figure 14. A vertical cross section of the 3D time constant model recovered from 3D inversion of the pole–dipole IP data along Line 1.

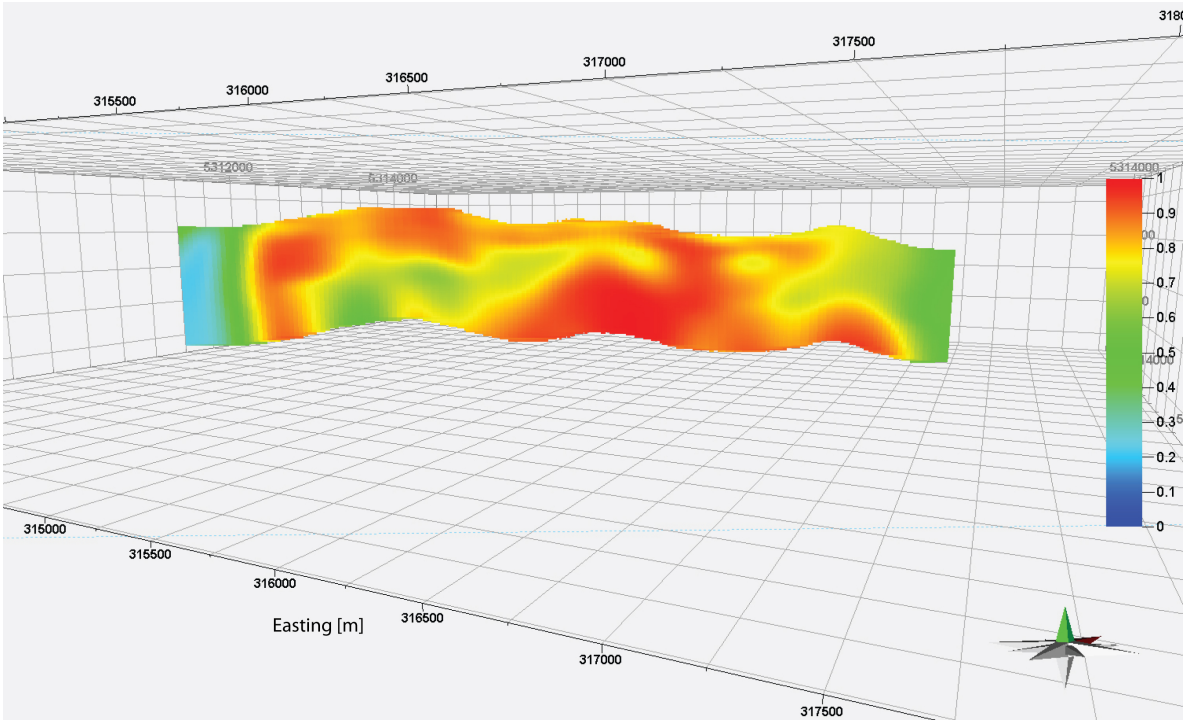

Figure 15. A vertical cross section of the 3D relaxation parameter model recovered from 3D inversion of the pole–dipole IP data along Line 1.

8.2. Interpretation of the Target Mineralization Zones

We have interpreted the target mineralization zones by using geoelectrical models recovered from 3D inversion of the IP data, petrophysical and mineralogical analyses of the rock samples [16], and assay data analysis of the drill cores. Based on the analyses of six rock samples with a relatively high grade of Cu (>0.1 %), we determined the ranges of electrical properties of the rocks (resistivity, chargeability, time constant, and relaxation parameter), which were used as the "filters" for the same parameters defined by 3D inversion.

Figure 16 shows the 3D cross plots between chargeability, time constant, and relaxation parameter, obtained from GEMTIP analysis of the rock samples. In this figure, the volume shown in red is assumed to represent the ranges of the electrical properties for the mineralized rock.

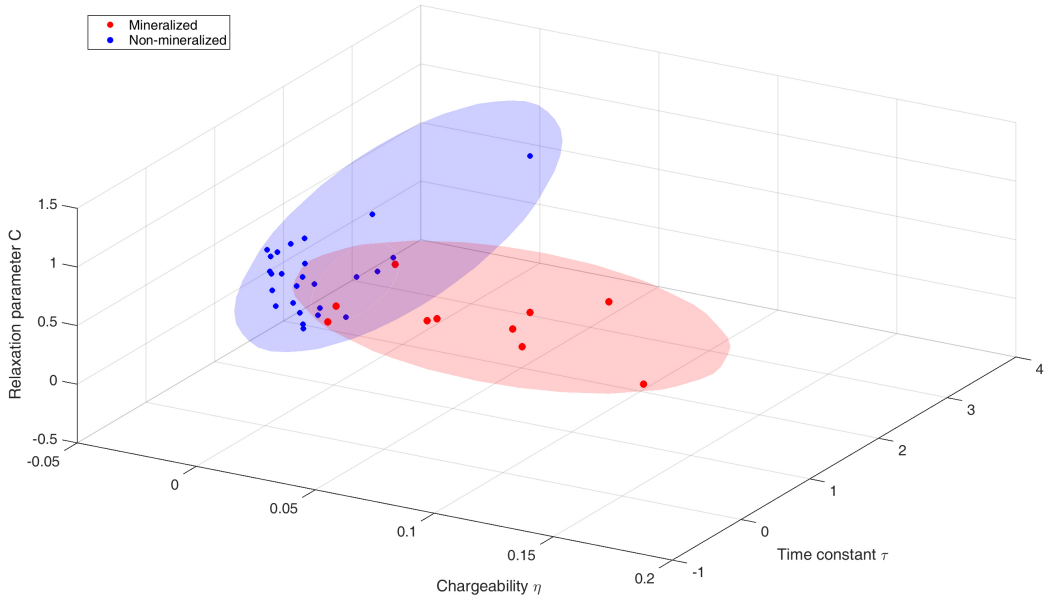

Figure 16. A 3D cross plot between the chargeability, time constant, and relaxation parameter. The target mineralized zones can be specified using the range of red volume.

Figures 17 and 18 show a 3D view and top view of the interpreted target mineralized zones. In those figures, the color of the body corresponds to the chargeability value recovered from the 3D inversion of the IP data (hot color—high chargeability; cold color—low chargeability). Figure 19 show vertical cross sections of the interpreted target mineralized zones along the five lines shown in Figure 18. One can clearly see good correlations between the interpreted bodies and known mineralization. This opens a possibility to estimate the target mineralized zones by using a rigorous 3D inversion of the IP data interpreted with petrophysical and mineralogical analyses of rock samples, and assay data analysis.

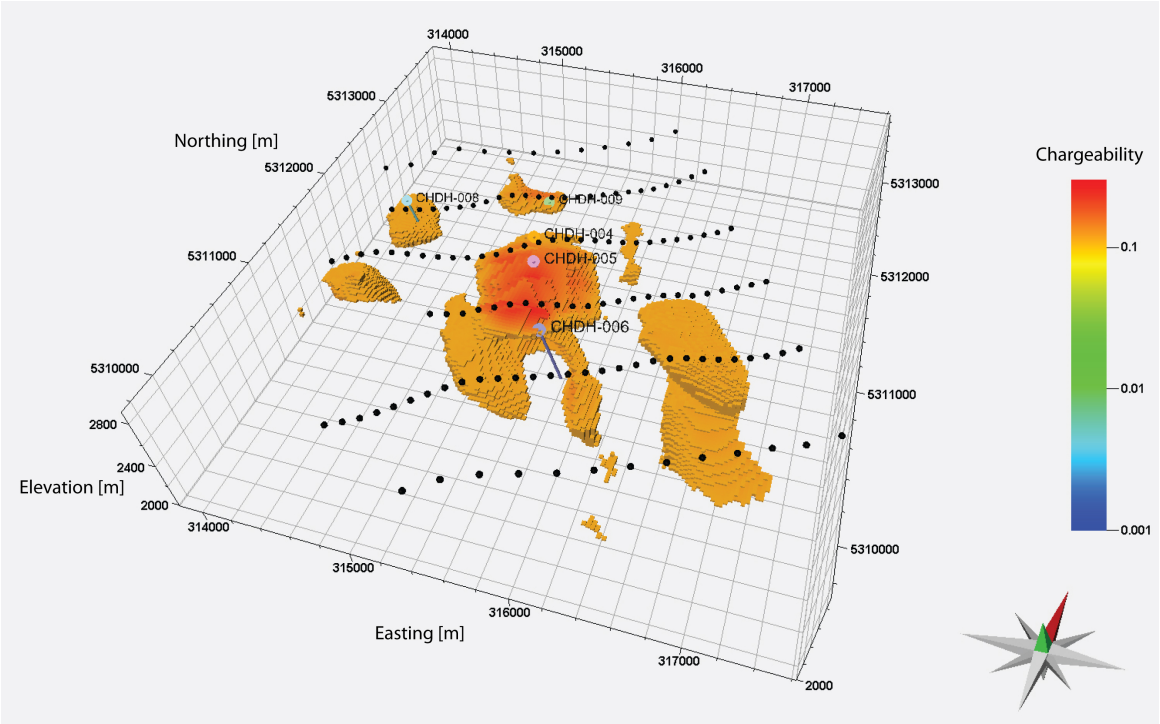

Figure 17. A 3D view of the interpreted target mineralized zones.

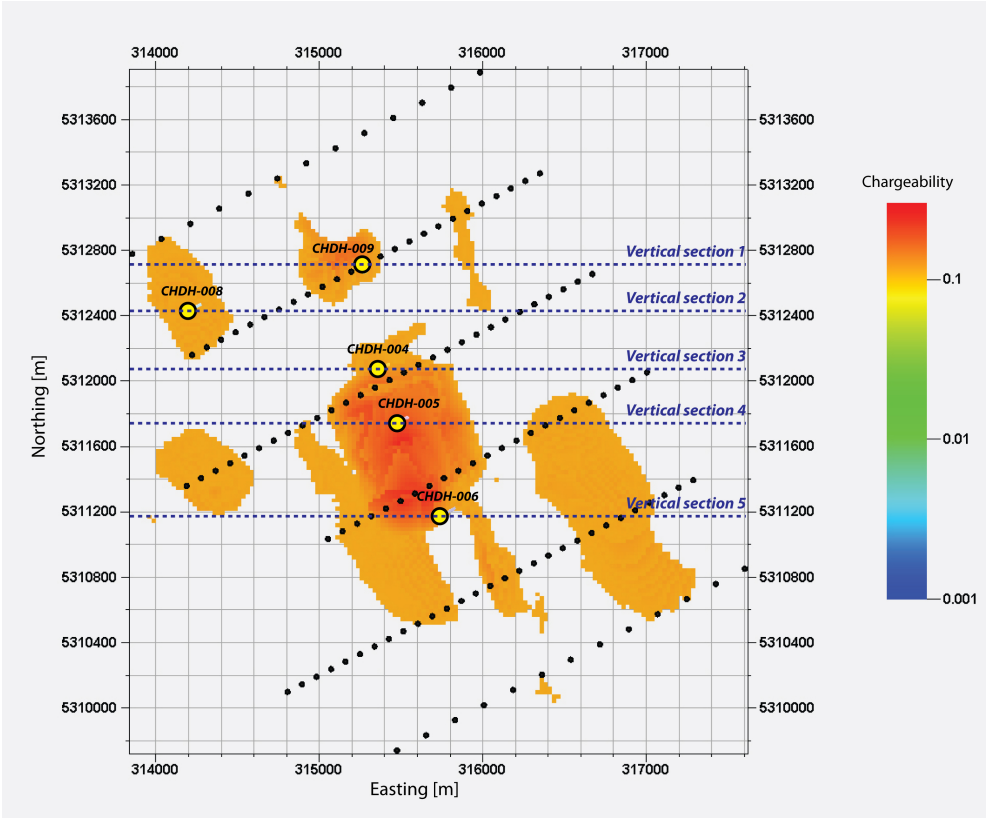

Figure 18. A top view of the interpreted target mineralized zones.

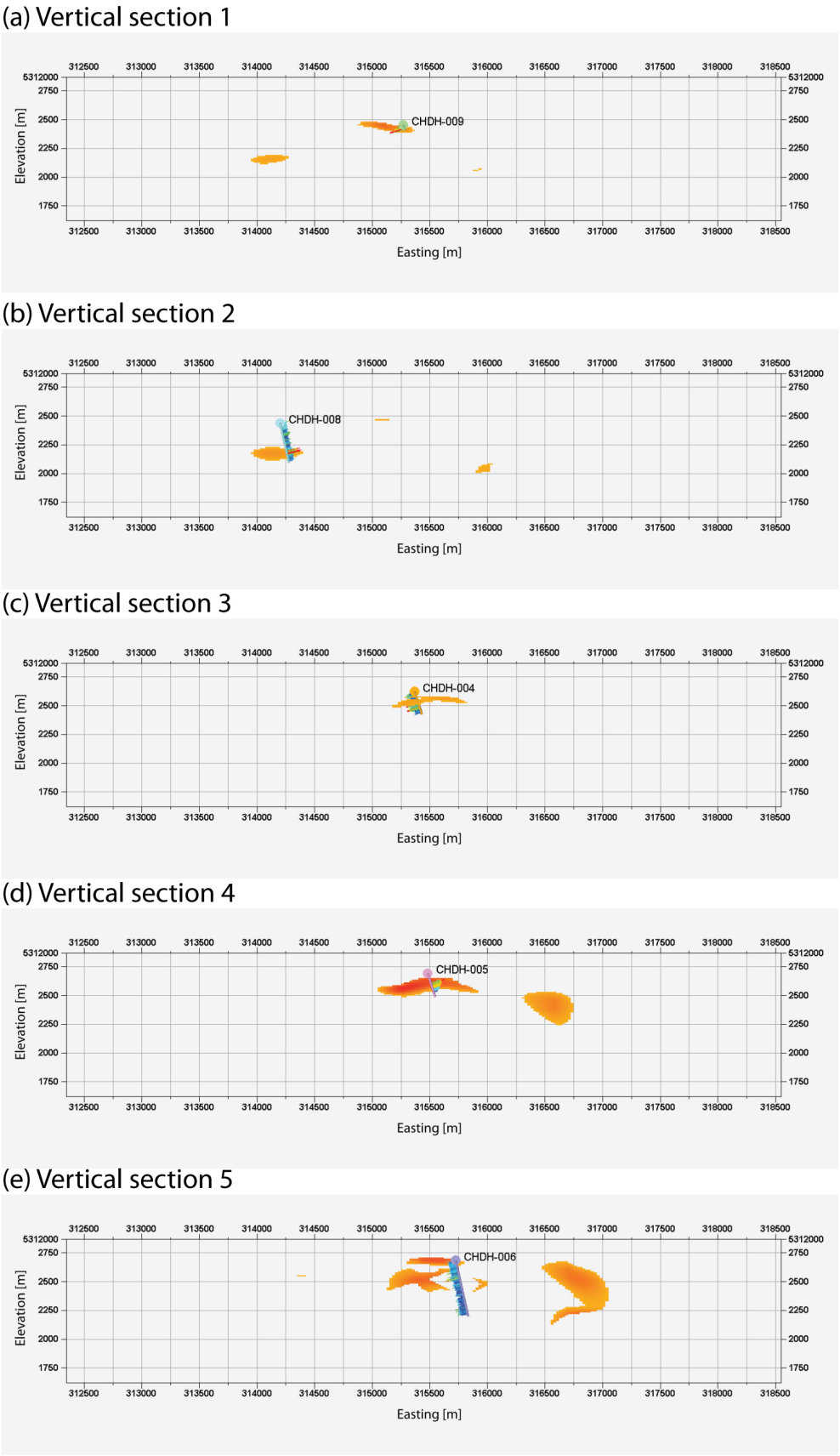

Figure 19. Vertical cross sections of the 3D interpreted target mineralized zones along (**a**) section 1, (**b**) section 2, (**c**) section 3, (**d**) section 4, and (**e**) section 5 in Figure 18, with assay data.

9. Conclusions

We have developed a novel method of 3D inversion of the IP data based on the GEMTIP conductivity relaxation model. The developed method takes into account the nonlinear nature of both the electromagnetic induction and the IP phenomena and inverts the EM data into the parameters of the GEMTIP model. The method was validated by synthetic data inversions of both frequency and time domain IP data for the GEMTIP model parameters. We have applied the developed method to the 3D inversion of the IP data acquired in Mongolia.

We have also established a workflow for comprehensive interpretation of IP survey data by integrating our developed rigorous 3D inversion technique with the results of petrophysical and mineralogical analysis of rock samples, and with the results of assay data analysis. It was demonstrated that our interpretation workflow can estimate the target mineralized zones appropriately, and this opens a possibility to estimate the target mineralized zones remotely.

Acknowledgments: The authors acknowledge the Consortium for Electromagnetic Modeling and Inversion (CEMI) and TechnoImaging for support of this project and permission to publish. We are thankful to the First Eurasian Mining LC for providing the IP survey data and rock samples.

Author Contributions: Michael Zhdanov has contributed overall scientific development including the development of the theory of GEMTIP model and regularized 3D inversion. Masashi Endo has managed the research project, and contributed comprehensive interpretation. Leif Cox and David Sunwall have developed the 3D inversion code, and applied it to the synthetic and real field IP data.

Conflicts of Interest: The authors declare no conflict of interest.

References

1. Zonge, K.L.; Wynn, J.C. Recent advances and applications in complex resistivity measurements. *Geophysics* **1975**, *40*, 851–864.
2. Pelton, W.H.; Smith, B.D.; Sill, W.R. Inversion of complex resistivity and dielectric data. *Geophysics* **1975**, *40*, 153.
3. Pelton, W.H.; Rijo, L.; Swift, C.M., Jr. Inversion of two-dimensional resistivity and induced-Polarization data. *Geophysics* **1978**, *43*, 788–803.
4. Pelton, W.H.; Ward, S.H.; Hallof, P.G.; Sill, W.R.; Nelson, P.H. Mineral discrimination and removal of inductive coupling with multifrequency IP. *Geophysics* **1978**, *43*, 547–565.
5. Li, Y.; Oldenburg, D.W. Inversion of 3D DC resistivity data using an approximate inverse mapping. *Geophys. J. Int.* **1994**, *116*, 527–537.
6. Li, Y.; Oldenburg, D.W. 3-D inversion of induced polarization data. *Geophysics* **2000**, *65*, 1931–1945.
7. Cole, K.S.; Cole, R.H. Dispersion and absorption in dielectrics. *J. Chem. Phys.* **1941**, *9*, 343–351.
8. Pelton, W.H. Interpretation of Induced Polarization and Resistivity Data. Ph.D. Thesis, University of Utah, Salt Lake City, UT, USA, 1977.
9. Yuval, D.; Oldenburg, D.W. Computation of Cole-Cole parameters from IP data. *Geophysics* **1997**, *62*, 436–448.
10. Routh, P.S.; Oldenburg, D.W. Electromagnetic coupling in frequency-domain induced polarization data: A method for removal. *Geophys. J. Int.* **2001**, *145*, 59–76.
11. Rowston, P.; Busuttil, S.; McNeill, G. Cole-Cole inversion telluric cancelled IP data. *ASEG Ext. Abstr.* **2003**, *2003*, 1–4.
12. Yoshioka, K.; Zhdanov, M.S. Three-dimensional nonlinear regularized inversion of the induced polarization data based on the Cole–Cole model. *Phys. Earth Planet. Inter.* **2005**, *150*, 29–43.
13. Zhang, W.; Liu, J.-X.; Guo, Z.-W.; Tong, X.-Z. Cole-Cole model based on the frequency-domain IP method of forward modeling. In Proceedings of the Progress in Electromagnetics Research Symposium, Xi'an, China, 22–26 March 2010; pp. 383–386.
14. Zhdanov, M.S. Generalized effective-medium theory of induced polarization. *Geophysics* **2008**, *73*, F197–F211.
15. Xu, Z.; Zhdanov, M.S. Three-dimensional Cole-Cole model inversion of induced polarization data based on regularized conjugate gradient method. *IEEE Geosci. Remote Sens. Lett.* **2015**, *12*, 1180–1184.

16. Zhdanov, M.S.; Burtman, V.; Endo, M.; Lin, W. Complex resistivity of mineral rocks in the context of the generalized effective-medium theory of the induced polarization effect. *Geophys. Prospect.* **2017**, doi:10.1111/1365-2478.12581.
17. Zhdanov, M.S. *Foundations of Geophysical Electromagnetic Theory and Methods*; Elsevier: Amsterdam, The Netherlands, 2017.
18. Zhdanov, M.S. *Geophysical Inverse Theory and Regularization Problems*; Elsevier: Amsterdam, The Netherlands, 2002.
19. Zhdanov, M.S. *Inverse Theory and Applications in Geophysics*; Elsevier: Amsterdam, The Netherlands, 2015.
20. Zhdanov, M.S. *Geophysical Electromagnetic Theory and Methods*; Elsevier: Amsterdam, The Netherlands, 2009.
21. Gribenko, A.; Zhdanov, M.S. Rigorous 3D inversion of marine CSEM data based on the integral equation method. *Geophysics* **2007**, *72*, 229–254.
22. Tikhonov, A.N.; Arsenin, V.Y. *Solutions of Ill-Posed Problems*; Wiley: Hoboken, NJ, USA, 1977.

© 2018 by the authors. Licensee MDPI, Basel, Switzerland. This article is an open access article distributed under the terms and conditions of the Creative Commons Attribution (CC BY) license (http://creativecommons.org/licenses/by/4.0/).